



PERGAMON

Available online at www.sciencedirect.com

SCIENCE @ DIRECT®

International Journal of Heat and Mass Transfer 46 (2003) 5113–5121

International Journal of
**HEAT and MASS
TRANSFER**

www.elsevier.com/locate/ijhmt

Turbulent flow in a channel occupied by a porous layer considering the stress jump at the interface

Renato A. Silva, Marcelo J.S. de Lemos *

Departamento de Energia, IEME, Instituto Tecnológico de Aeronáutica, ITA-CTA, 12228-900 São José dos Campos, SP, Brazil

Received 12 December 2002; received in revised form 18 June 2003

Abstract

For hybrid media, involving both a porous structure and a clear flow region, difficulties arise due to the proper mathematical treatment given at the interface. The literature proposes a jump condition in which shear stresses on both sides of the interface are not of the same value. This paper presents numerical solutions for such hybrid medium, considering here a channel partially filled with a porous layer through which fluid flows in turbulent regime. One unique set of transport equations is applied to both regions. Effects of Reynolds number, porosity, permeability and jump coefficient on mean and turbulence fields are investigated. Results indicate that depending on the value of the stress jump parameters, a substantially different structure for the turbulent field is obtained.

© 2003 Elsevier Ltd. All rights reserved.

Keywords: Turbulence modeling; Porous media; Volume-average; Time-average; Interface; Stress jump

1. Introduction

Environmental flows of extreme importance, such as turbulent atmospheric boundary layer over thick rain forests, may benefit from more realistic mathematical models. Accordingly, flow over layers of dense vegetation can be characterized by some sort of porous structure through which a fluid permeates.

Traditionally, volume-average properties for an homogenous treatment of flow in porous media are obtained by means of the volume-average theorem (VAT) [1,2]. When the domain presents a macroscopic interfacial area, the literature proposes the existence of a stress jump interface condition between the clear flow region and the porous medium [3,4].

Purely numerical solutions for two-dimensional hybrid medium (porous region–clear flow) in an isothermal channel has been considered in [5] based on the turbu-

lence model proposed in [6,7]. That work has been developed under the double-decomposition concept [8–10]. Non-isothermal flows in channels past a porous obstacle [11] and through a porous insert have also been presented [12]. In all previous work of [5,11,12], the interface boundary condition considered a continuous function for the stress field across the interface.

Recently, the interface jump condition has been investigated for laminar flows, either considering non-linear effects in momentum equation [13] as well as neglecting the Forchheimer term in the macroscopic model [14]. Such works were based on the numerical methodology proposed for hybrid media and applied by [5,11,12]. In [15], a detailed numerical model for including the interface jump condition was presented. Therein, the authors simulated laminar flow over such interfaces and validated their results against analytical solutions by [16–18].

The objective of this paper is to extend the work of [19] for laminar flows computing now turbulent regime. Flows parallel to interfaces between a porous medium and a clear fluid are computed considering the mathematical treatment given by [3,4].

* Corresponding author. Tel.: +55-12-3947-5860; fax: +55-12-3947-5842.

E-mail address: delemos@mec.ita.br (M.J.S. de Lemos).

Nomenclature

c_F	Forchheimer coefficient in Eq. (4)
c_1, c_2	constants in Eq. (9)
c_k	constant in Eq. (8)
c_μ	constant in Eq. (7)
Da	Darcy number, $Da = K/H^2$
\mathbf{D}	deformation rate tensor, $\mathbf{D} = [\nabla\mathbf{u} + (\nabla\mathbf{u})^T]/2$
d	particle or pore diameter
G^i	production rate of k due to the porous matrix, $G^i = c_k \rho \phi \langle k \rangle^i \bar{\mathbf{u}}_D / \sqrt{K}$
H	distance between channel walls
\mathbf{I}	unit tensor
k	turbulent kinetic energy per unit mass, $k = \overline{\mathbf{u}' \cdot \mathbf{u}'}/2$
$\langle k \rangle^V$	volume (fluid + solid) average of k
$\langle k \rangle^i$	intrinsic (fluid) average of k
K	permeability
L	axial length of periodic section of channel
p	thermodynamic pressure
$\langle p \rangle^i$	intrinsic (fluid) average of pressure p
P^i	production rate of k due to mean gradients of $\bar{\mathbf{u}}_D$, $P^i = -\rho \langle \overline{\mathbf{u}'\mathbf{u}'} \rangle^i : \nabla \bar{\mathbf{u}}_D$
$\bar{\mathbf{R}}$	time average of total drag per unit volume
Re_H	Reynolds number based on the channel height, $Re_H = \frac{\rho \bar{\mathbf{u}}_D H}{\mu}$
s	clearance for unobstructed flow

S_ϕ	source term
$\bar{\mathbf{u}}$	microscopic time-averaged velocity vector
$\langle \bar{\mathbf{u}} \rangle^i$	intrinsic (fluid) average of $\bar{\mathbf{u}}$
$\bar{\mathbf{u}}_D$	Darcy velocity vector, $\bar{\mathbf{u}}_D = \phi \langle \bar{\mathbf{u}} \rangle^i$
$\bar{\mathbf{u}}_{D_i}$	Darcy velocity vector at the interface
$\bar{\mathbf{u}}_{D_p}$	Darcy velocity vector parallel to the interface
u_{D_n}, u_{D_p}	components of Darcy velocity at interface along η (normal) and ζ (parallel) directions, respectively
u_{D_i}, v_{D_i}	components of Darcy velocity at interface along x and y , respectively
x, y	Cartesian coordinates

Greek symbols

β	interface stress jump coefficient
μ	fluid dynamic viscosity
μ_{eff}	effective viscosity for a porous medium
μ_ϕ	macroscopic turbulent viscosity
ε	dissipation rate of k , $\varepsilon = \mu \nabla \mathbf{u}' : (\nabla \mathbf{u}')^T / \rho$
$\langle \varepsilon \rangle^i$	intrinsic (fluid) average of ε
ρ	density
ϕ	porosity
Φ	general dependent variable
η, ζ	generalized coordinates

2. Macroscopic mathematical model

2.1. Geometry and governing equations

The flow under consideration is schematically shown in Fig. 1 where a channel is partially filled with a layer of a porous material. A constant property fluid flows longitudinally from left to right permeating through both the clear region and the porous structure. The case in Fig. 1 uses symmetry boundary condition at the channel center ($y = 0$). Also, $H = 10$ cm is the distance in between the channel walls and s the clearance for the non-obstructed flow passage. It should be emphasized that the class of flow under consideration involves porous substrates having a high porosity and permeability. Shell and tube heat exchangers [20] and a nuclear reactor core [21], for example, can be seen as porous structures with the fluid phase flowing in turbulent regime.

A macroscopic form of the governing equations is obtained by taking the volumetric average of the entire equation set. In this development, the porous medium is considered to be rigid and saturated by the incompressible fluid.

The macroscopic continuity equation is given by,

$$\nabla \cdot \bar{\mathbf{u}}_D = 0 \quad (1)$$

where the Dupuit–Forchheimer relationship, $\bar{\mathbf{u}}_D = \phi \langle \bar{\mathbf{u}} \rangle^i$, has been used and $\langle \bar{\mathbf{u}} \rangle^i$ identifies the intrinsic (liquid) average of the local velocity vector $\bar{\mathbf{u}}$ [2]. Eq. (1) represents the macroscopic continuity equation for an incompressible fluid in a rigid porous medium.

The macroscopic time-mean Navier–Stokes (NS) equation for an incompressible fluid with constant properties can be written as,

$$\rho \left[\frac{\partial}{\partial t} (\phi \langle \bar{\mathbf{u}} \rangle^i) + \nabla \cdot (\phi \langle \bar{\mathbf{u}}\bar{\mathbf{u}} \rangle^i) \right] = -\nabla (\phi \langle \bar{p} \rangle^i) + \mu \nabla^2 (\phi \langle \bar{\mathbf{u}} \rangle^i) + \nabla \cdot (-\rho \phi \langle \overline{\mathbf{u}'\mathbf{u}'} \rangle^i) + \bar{\mathbf{R}} \quad (2)$$

As usually done when treating turbulence with statistical tools, the correlation $-\rho \overline{\mathbf{u}'\mathbf{u}'}$ appears after application of the time-average operator to the local instantaneous NS equation. Applying further the volume-average procedure to the entire momentum equation (see [6] for details), results in the term $-\rho \phi \langle \overline{\mathbf{u}'\mathbf{u}'} \rangle^i$ of (2). This term is here recalled as the macroscopic Reynolds stress tensor (MRST). In addition, $\bar{\mathbf{R}}$ in (2) represents the time-mean

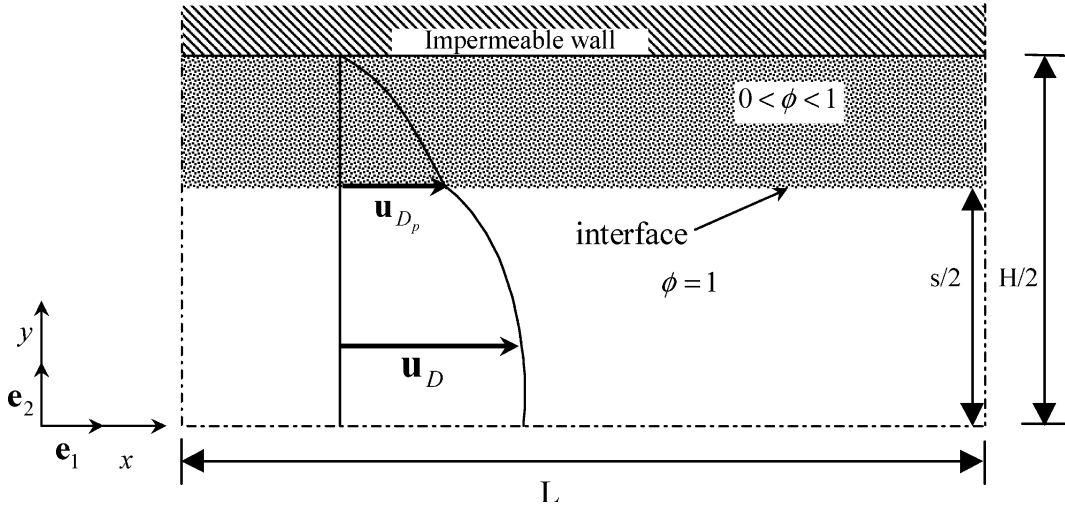


Fig. 1. Model for turbulent channel flow with porous material.

total drag per unit volume acting on the fluid by the action of the porous structure. A common model for it is known as the Darcy–Forchheimer extended model and is given by:

$$\bar{\mathbf{R}} = - \left[\frac{\mu\phi}{K} \bar{\mathbf{u}}_D + \frac{c_F \phi \rho |\bar{\mathbf{u}}_D| \bar{\mathbf{u}}_D}{\sqrt{K}} \right] \quad (3)$$

where the constant c_F is known in the literature as the non-linear Forchheimer coefficient.

Then, making use again of the expression $\bar{\mathbf{u}}_D = \phi \langle \bar{\mathbf{u}} \rangle^i$ and (3), Eq. (2) can be rewritten as,

$$\begin{aligned} \rho \left[\frac{\partial \bar{\mathbf{u}}_D}{\partial t} + \nabla \cdot \left(\frac{\bar{\mathbf{u}}_D \bar{\mathbf{u}}_D}{\phi} \right) \right] \\ = -\nabla \cdot (\phi \langle \bar{p} \rangle^i) + \mu \nabla^2 \bar{\mathbf{u}}_D + \nabla \cdot \left(-\rho \phi \langle \bar{\mathbf{u}} \bar{\mathbf{u}} \rangle^i \right) \\ - \left[\frac{\mu\phi}{K} \bar{\mathbf{u}}_D + \frac{c_F \phi \rho |\bar{\mathbf{u}}_D| \bar{\mathbf{u}}_D}{\sqrt{K}} \right] \end{aligned} \quad (4)$$

Further, a model for the MRST in analogy with the Boussinesq concept for clear fluid can be written as:

$$-\rho \phi \langle \bar{\mathbf{u}} \bar{\mathbf{u}} \rangle^i = \mu_{t_\phi} 2 \langle \bar{\mathbf{D}} \rangle^v - \frac{2}{3} \phi \rho \langle k \rangle^i \mathbf{I} \quad (5)$$

where

$$\langle \bar{\mathbf{D}} \rangle^v = \frac{1}{2} [\nabla \cdot (\phi \langle \bar{\mathbf{u}} \rangle^i) + [\nabla \cdot (\phi \langle \bar{\mathbf{u}} \rangle^i)]^T] \quad (6)$$

is the macroscopic deformation tensor, $\langle k \rangle^i$ is the intrinsic average for k and μ_{t_ϕ} is the macroscopic turbulent viscosity. The macroscopic turbulent viscosity, μ_{t_ϕ} , used in (5) is modeled similarly to the case of clear fluid flow and a proposal for it was presented in [6] as,

$$\mu_{t_\phi} = \rho c_\mu \langle k \rangle^i / \langle \varepsilon \rangle^i \quad (7)$$

2.2. Macroscopic equations for $\langle k \rangle^i$ and $\langle \varepsilon \rangle^i$

Transport equations for $\langle k \rangle^i = \langle \bar{\mathbf{u}} \cdot \bar{\mathbf{u}} \rangle^i / 2$ and $\langle \varepsilon \rangle^i = \mu \langle \nabla \mathbf{u}' : (\nabla \mathbf{u}')^T \rangle^i / \rho$ in their so-called high Reynolds number form are proposed in [6] as:

$$\begin{aligned} \rho \left[\frac{\partial}{\partial t} (\phi \langle k \rangle^i) + \nabla \cdot (\bar{\mathbf{u}}_D \langle k \rangle^i) \right] \\ = \nabla \cdot \left[\left(\mu + \frac{\mu_{t_\phi}}{\sigma_k} \right) \nabla (\phi \langle k \rangle^i) \right] + P^i + G^i - \rho \phi \langle \varepsilon \rangle^i \end{aligned} \quad (8)$$

where $P^i = -\rho \langle \bar{\mathbf{u}} \bar{\mathbf{u}} \rangle^i : \nabla \bar{\mathbf{u}}_D$, $G^i = c_k \rho \frac{\phi \langle k \rangle^i |\bar{\mathbf{u}}_D|}{\sqrt{K}}$ and

$$\begin{aligned} \rho \left[\frac{\partial}{\partial t} (\phi \langle \varepsilon \rangle^i) + \nabla \cdot (\bar{\mathbf{u}}_D \langle \varepsilon \rangle^i) \right] \\ = \nabla \cdot \left[\left(\mu + \frac{\mu_{t_\phi}}{\sigma_\varepsilon} \right) \nabla (\phi \langle \varepsilon \rangle^i) \right] \\ + c_1 P^i \frac{\langle \varepsilon \rangle^i}{\langle k \rangle^i} + c_2 \frac{\langle \varepsilon \rangle^i}{\langle k \rangle^i} (G^i - \rho \phi \langle \varepsilon \rangle^i) \end{aligned} \quad (9)$$

where c_1 , c_2 and c_k are constants, P^i is the production rate of $\langle k \rangle^i$ due to gradients of $\bar{\mathbf{u}}_D$ and G^i the generation rate of the intrinsic average of k due to the action of the porous matrix.

2.3. Interface and boundary conditions

The equation proposed in [3,4] for describing the stress jump at the interface between the clear flow region and the porous structure is given by,

$$\begin{aligned} \mu_{\text{eff}} \frac{\partial u_{D_p}}{\partial \eta} \Big|_{\text{Porous medium}} - \mu \frac{\partial u_{D_p}}{\partial \eta} \Big|_{\text{Clear fluid}} \\ = \beta \frac{\mu}{\sqrt{K}} u_{D_p} \Big|_{\text{Interface}} \end{aligned} \quad (10)$$

where u_{Dp} is the Darcy velocity component parallel to the interface (see Fig. 1), μ_{eff} is the effective viscosity for the porous region, μ is the fluid dynamic viscosity, K is the permeability and β an adjustable coefficient which accounts for the stress jump at the interface.

It is important to emphasize that the macroscopic model for the interface here employed makes no assumption about the topology of the surface, nor is this interface the one existing in transpired solid walls, for example. Or say, although the microscopic interfacial area surrounding the irregular geometry of solid particles facing the clear medium may be characterized by statistical values, such as an average thickness or roughness, in the present macroscopic view no such thickness or roughness is associated with the interface. In fact, in Kaviani [22, p. 71], the order of magnitude of the roughness of the interface is of order of d (pore/particle diameter), which is much higher than \sqrt{K} , another length associated with permeable media. Had the interface roughness been considered, that would be of the order of d , the mean particle/pore diameter. Here, irregular or rough boundaries between the porous medium and the clear fluid are treated under the macroscopic view and, as such, no statistical value of interface thickness is attributed to the modeled surface separating the two media. Likewise, transpired walls made of a porous substrate with extremely small porous sizes are here not treated. Also, the macroscopic velocity at the interface and on its surroundings is assumed to be of sufficient value so that a viscous sublayer similar to the one existing over impermeable surfaces are not present in the context herein.

In addition to Eq. (10), continuity of velocity, pressure, statistical variables and their fluxes across the interface are given by,

$$\bar{u}_D|_{0<\phi<1} = \bar{u}_D|_{\phi=1} \quad (11)$$

$$\langle \bar{p} \rangle^i|_{0<\phi<1} = \langle \bar{p} \rangle^i|_{\phi=1} \quad (12)$$

$$\langle k \rangle^v|_{0<\phi<1} = \langle k \rangle^v|_{\phi=1} \quad (13)$$

$$\left(\mu + \frac{\mu_{t\phi}}{\sigma_k} \right) \frac{\partial \langle k \rangle^v}{\partial y} \Big|_{0<\phi<1} = \left(\mu + \frac{\mu_t}{\sigma_k} \right) \frac{\partial \langle k \rangle^v}{\partial y} \Big|_{\phi=1} \quad (14)$$

$$\langle \varepsilon \rangle^v|_{0<\phi<1} = \langle \varepsilon \rangle^v|_{\phi=1} \quad (15)$$

$$\left(\mu + \frac{\mu_{t\phi}}{\sigma_\varepsilon} \right) \frac{\partial \langle \varepsilon \rangle^v}{\partial y} \Big|_{0<\phi<1} = \left(\mu + \frac{\mu_t}{\sigma_\varepsilon} \right) \frac{\partial \langle \varepsilon \rangle^v}{\partial y} \Big|_{\phi=1} \quad (16)$$

Further, the extension of (10) to the case of turbulent flow can be given as,

$$\begin{aligned} & (\mu_{\text{eff}} + \mu_{t\phi}) \frac{\partial \bar{u}_{Dp}}{\partial y} \Big|_{0<\phi<1} - (\mu + \mu_t) \frac{\partial \bar{u}_{Dp}}{\partial y} \Big|_{\phi=1} \\ & = (\mu + \mu_t) \frac{\beta}{\sqrt{K}} \bar{u}_{D1} \Big|_{\text{Interface}} \end{aligned} \quad (17)$$

Eqs. (11) and (12) were also proposed in [3,4] whereas relationships (13)–(15), (17) were used by [23].

Before proceeding, a word about the use of expression (10) seems timely. In Ochoa-Tapia and Whitaker [3,4] such an equation was proposed in order to accommodate a possible discontinuity in the diffusion flux of momentum across the interface. This model has already been applied to laminar flows involving analytical [16–18] and purely numerical solutions [19]. As already mentioned, an extension to turbulent has also been published [23], which adopted the continuity of diffusion fluxes for u_D (without any stress jump), for $\langle k \rangle^v$ (Eq. (14)), as well as for $\langle \varepsilon \rangle^v$ (condition (16)). When the right hand side of Eq. (10) is equal to zero, or say, when no stress jump is accounted for by setting $\beta = 0$, for example, one has a matching of diffusion fluxes across the interface, much like Eqs. (14) and (16) for $\langle k \rangle^v$ and $\langle \varepsilon \rangle^v$, respectively. Or say, due to the fact that a second derivative exists in expressions, (4), (8) and (9), it is possible, but not mandatory, that diffusion fluxes match at the interface (see [22], p. 92). Had a similar “jump” been considered in order to account for some extra effect in the $\langle k \rangle^v$ -equation, for example, we would have had an interface condition of the form:

$$\begin{aligned} & \left(\mu + \frac{\mu_{t\phi}}{\sigma_k} \right) \frac{\partial \langle k \rangle^v}{\partial y} \Big|_{0<\phi<1} - \left(\mu + \frac{\mu_t}{\sigma_k} \right) \frac{\partial \langle k \rangle^v}{\partial y} \Big|_{\phi=1} \\ & = [\text{jump term for } \langle k \rangle^v] \end{aligned} \quad (18)$$

instead of Eq. (14). Here, however, no such discontinuity on diffusion fluxes for the statistical quantities is assumed.

Also, standard wall functions have been employed for calculating the flow in the proximity of channel walls. Detailed information on such numerical treatment can be found in [6,7]. Justification for using such simpler treatment is twofold: (1) final velocity values close to the interface will be a function not only of the inertia and viscous effects in the full Navier–Stokes equation, but also due to the Darcy and Forchheimer resistance terms. Therefore, eventual errors coming from inaccurate use of a more appropriate boundary conditions will have little influence on the final value for the velocity close to the wall since drag forces, caused by the porous structure, will play also an important role in determining the final value for the wall velocity, (2) logarithm wall laws are simple to be incorporated when simulating flow over rigid surfaces and for that they have been modified to include surface roughness and to simulate flows over irregular surfaces at the bottom of rivers [24].

In addition, is it interesting to emphasize that the class of flows under consideration is akin to having a sequence of closely spaced grids in a flow with a flat macroscopic Darcy velocity profile. Mechanical energy is transformed into turbulence kinetic energy as the flow crosses and is perturbed by the porous matrix. This in-

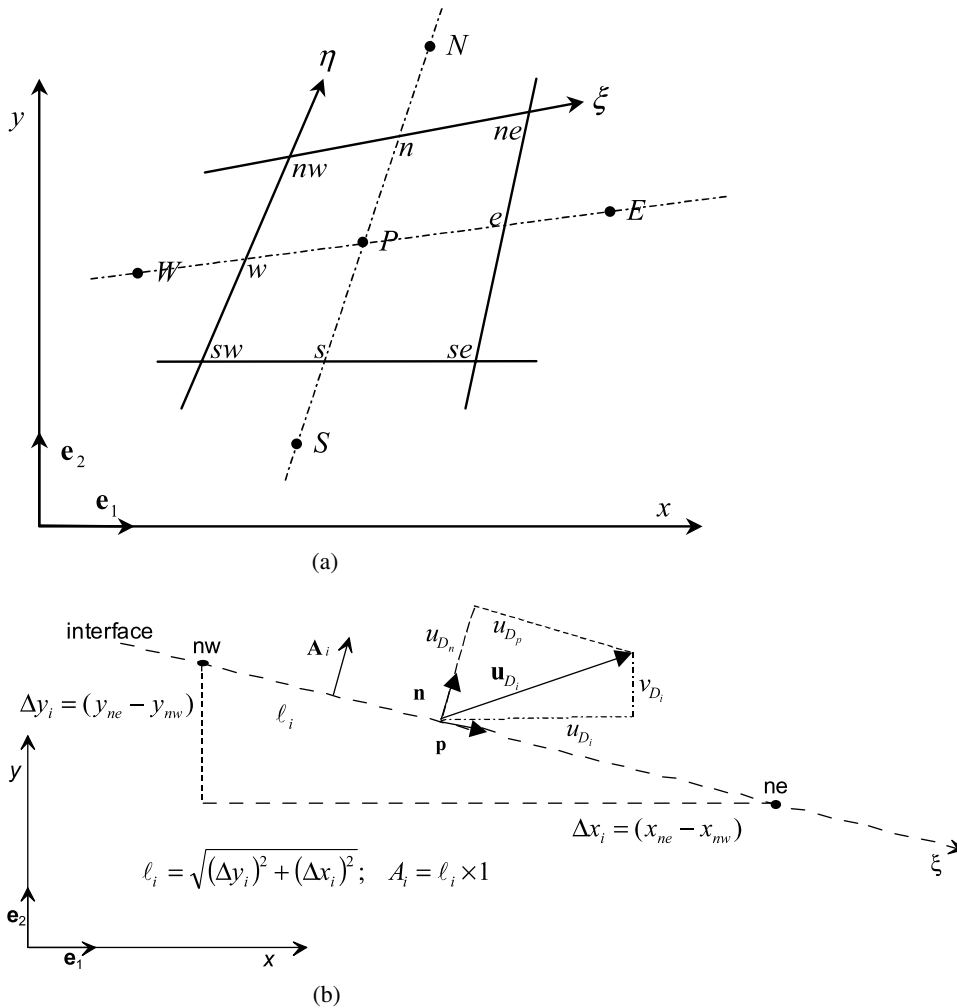


Fig. 2. Notation for (a) control volume discretization and (b) interface treatment.

terpretation of the model here used [6] has been detailed in de Lemos and Pedras [25].

Further, one should point out that condition (17) was first proposed by Ref. [23] and is valid along the macroscopic surface area dividing the clear and the porous regions. Application of the volume-average operators to a representative elementary volume [1,2] gives rise to terms such as the Darcy and Forchheimer flow resistances which, according to the literature [3,4,16–18], are not presented when analyzing macroscopic interfacial areas as here considered.

3. Numerical details

In an accompanying paper by [19], the discretization methodology used for including the jump condition in the numerical solutions was discussed in details. For

that, only brief comments about the numerical procedure are here made.

Fig. 2a shows a general control volume in a two-dimensional configuration. The faces of the volume are formed by lines of constant coordinates η – ξ . The work in [19] was set up for solving one-dimensional laminar flows in the geometry of Fig. 1 and employed the spatially periodic boundary condition along the x -coordinate. This was done in order to simulate fully developed flow. The spatially periodic condition was implemented by running the 2D solution repetitively, until outlet profiles in $x=L$ matched those at the inlet ($x=0$). Details on the methodology here employed for simulating fully developed flow using a two-dimensional numerical tool and the periodic condition along the x -direction can be found in [7,26,27].

For steady-state, a general form of the discrete equations for a general variable ϕ becomes,

$$I_e + I_w + I_n + I_s = S_\phi \tag{19}$$

where I_e , I_w , I_n and I_s are the fluxes of ϕ at faces *east*, *west*, *north* and *south* of the control volume of Fig. 2a, respectively, and S_ϕ is a source term. Here, all computations were carried out until normalized residues of the algebraic equations were brought down to 10^{-7} .

Fig. 2b shows details of the interface dividing two control volumes, one being located in the porous region and the other lying in the clear fluid. The computational grid based on generalized coordinate system η - ζ is such that the interface coincides with a line of constant η , extending itself along the ζ -coordinate. In this arrangement, the interface between the two neighbor volumes, each one located on each side of the interface, belongs to both faces of the two volumes. Thus, according to Fig. 2b, \bar{u}_D is the Darcy velocity at the interface and \bar{u}_{D_p} its component parallel to the interface.

The terms on the left of (17) were discretized according to the nomenclature shown in Fig. 2a. Details of such derivation can be found in [7] and for that they are not repeated here. Also, numerical details for the discretization of the right of (17) appears in [19].

4. Results and discussion

The flow in Fig. 1 was computed with the set of Eqs. (4), (8) and (9) with additional constitutive equation (5) and the Kolmogorov–Prandtl expression (7). Grid independence studies were conducted and for more than 40 nodal points in the cross-stream direction, the solution was essentially grid independent. The wall function approach was used for treating the flow close to the wall. One should emphasize that the numerical methodology

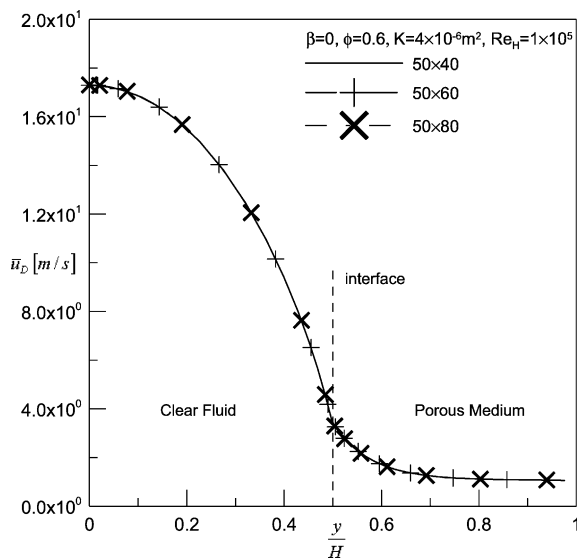
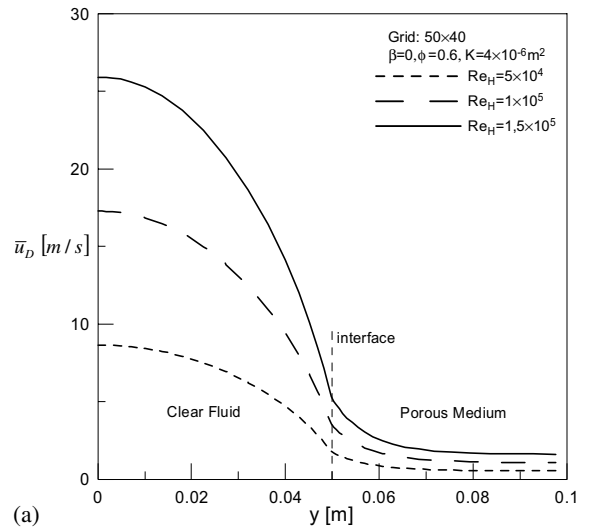
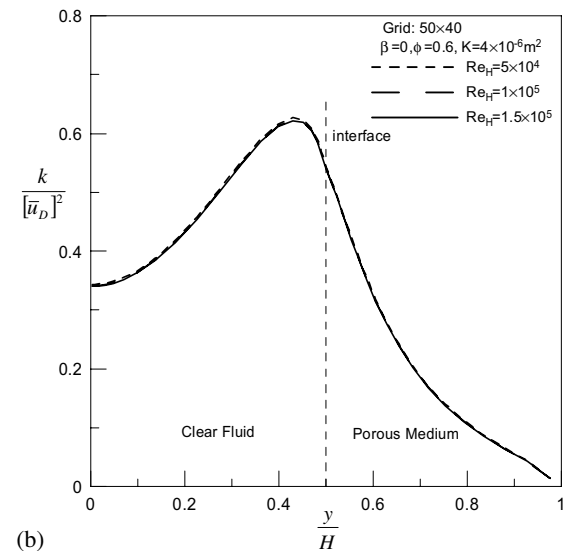


Fig. 3. Effect of mesh size on numerical solution.



(a)



(b)

Fig. 4. Effect of Reynolds number, Re_H , on macroscopic field: (a) mean velocity, (b) turbulent kinetic energy.

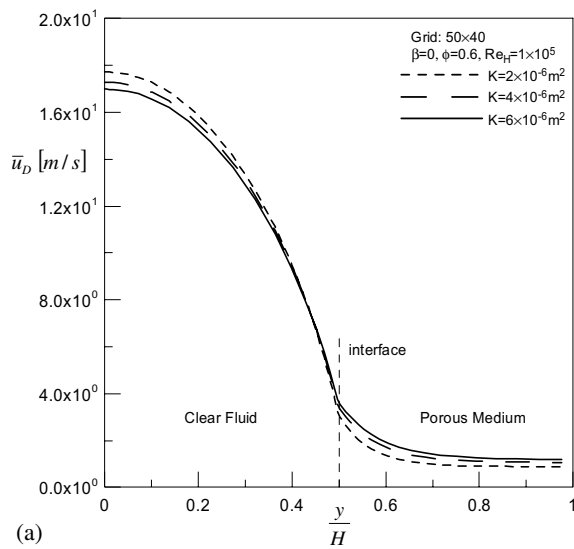
here considered was focused on two-dimensional flows, so that simulating the fully developed situation shown in the figure required the used of nodal points along the axial direction as well as the employment of the spatially periodic condition mentioned earlier. For all runs here studied, a total of 50 nodes in the axial direction was found to suffice. Also interesting to emphasize is that the sign of coefficient β in expression (10) will depend on the orientation of the y -axis in relation to the porous layer location. Here, the same orientation was used as the one given by Kuznetsov [16–18], which considers the porous layer at the top of the channel with its normal pointing towards the minus y -direction. As such, coherent computations for laminar flow were obtained [19]. Further,

grid independence studies were also carried out by Silva and de Lemos [19] indicating the proper size of the number of nodal points used around the interface. There, the authors correctly reproduced, with their numerical tool, the boundary layers around the interface proposed by the analytical study of Kuznetsov [16–18]. Also for the case of turbulent flow, as seen in Fig. 3, the number of grid point used seems to be appropriate.

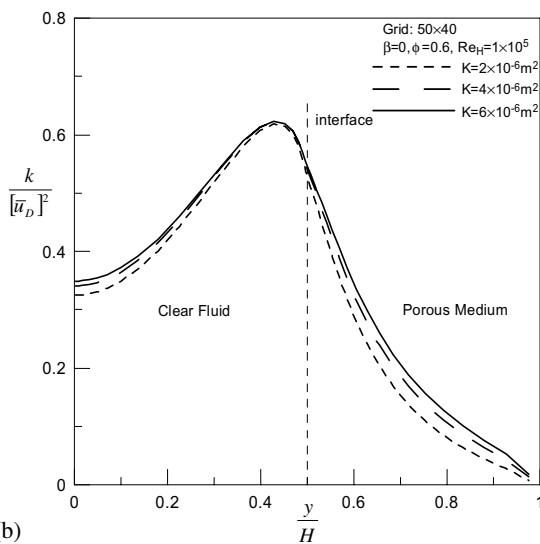
The effect of Re_H is shown in Fig. 4. The mean velocity in Fig. 4a indicates the increasing mass flow rate, within either the porous material or the clear passage, as the Reynolds increases. In Fig. 4b the collapse of curves for the turbulent kinetic energy divided by the mean mechanical energy shows that, for the range of Re_H

analyzed, the percentage of energy transformed into turbulence remains the same.

Fig. 5 shows the effect of the permeability K on both the mean and statistical fields. One can see that the greater the permeability, more flow crosses the porous substratum located in the region $0.5 < y/H < 1$ (Fig. 5a). The curves representing the statistical field in Fig. 5b show that, except close to the interface, the levels of k increase with increasing K . Within the clear fluid the production of turbulent kinetic energy is known to be dictated by gradients of the mean velocity (P^i on the right of (8)) whereas inside the permeable structure, the

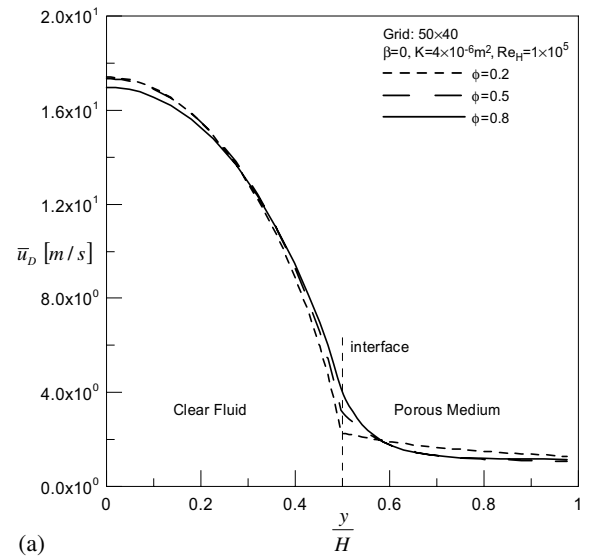


(a)

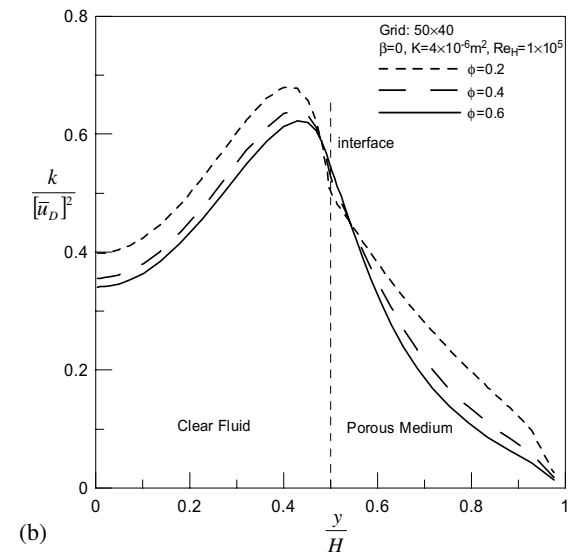


(b)

Fig. 5. Effect of permeability, K on macroscopic field: (a) mean velocity, (b) turbulent kinetic energy.



(a)



(b)

Fig. 6. Effect of porosity on macroscopic field: (a) mean velocity, (b) turbulent kinetic energy.

model of [6] proposes a factor proportional to \bar{u}_D as a generating mechanism for k (G^i in Eq. (8)).

Fig. 6a investigates the effect of the value of ϕ on the behavior of the mean velocity field. One can note that close to the interface, the greater the porosity, the higher the mass flow rate within the permeable layer. At the center of the channel, the velocity decreases in order to keep the imposed mass flow rate the same. It is interesting to observe that since the overall mass flow rate is forced to be constant, instead of the overall pressure loss along the channel, an increase in mass flow rate along the porous bed in the interface region is compensated by a slight re-

duction on local velocities close to the wall. Fig. 6b shows corresponding curves for the behavior of the turbulent kinetic energy. Away from the interface, values of k present a slight increase as ϕ is incremented. Greater values for the turbulence level within the porous layer ($y/H > 0.6$) are coherent with the model of Eq. (8) for the extra generation rate due to the porous matrix. As said, this extra G^i term (third on the right of (8)) was modeled as proportional to \bar{u}_D and, inside the porous layer ($y/H > 0.6$), the mean Darcy velocity increase as ϕ is reduced.

Fig. 7 finally presents numerical solutions for β varying from -0.5 to 0.5 for a fixed porosity $\phi = 0.6$, permeability $K = 4 \times 10^{-6} \text{ m}^2$ and $Re_H = 1 \times 10^5$. Profiles for \bar{u}_D change substantially as the factor β is varied, from a smooth variation across the interface for a negative β , to an abrupt change in the velocity profiles when $\beta > 0$. For positive values, the Darcy velocity \bar{u}_D is higher inside the permeable structure. In turn, turbulent kinetic energy is generated at a faster rate by the model proposed in Eq. (8). Although mean velocity profiles are flat in this same porous region, reducing the production rate P^i , the generating mechanism G^i increases the overall value of k . In the clear fluid, steeper gradients in the fluid layer also contributes for increasing the value of the turbulent kinetic energy. Then, either by P^i in the clear fluid or by G^i in the porous layer, turbulent kinetic energy is generated at a faster rate for positive values of β . Ultimately, results in Fig. 7 indicates that for flows where models with $\beta > 0$ are suitable, a greater portion of the mean mechanical energy of the flow is converted into turbulence. If that is the case of environmental flows over dense and thick rain forests, for example, results herein might be useful to environmentalists and engineers analyzing important natural and engineering flows.

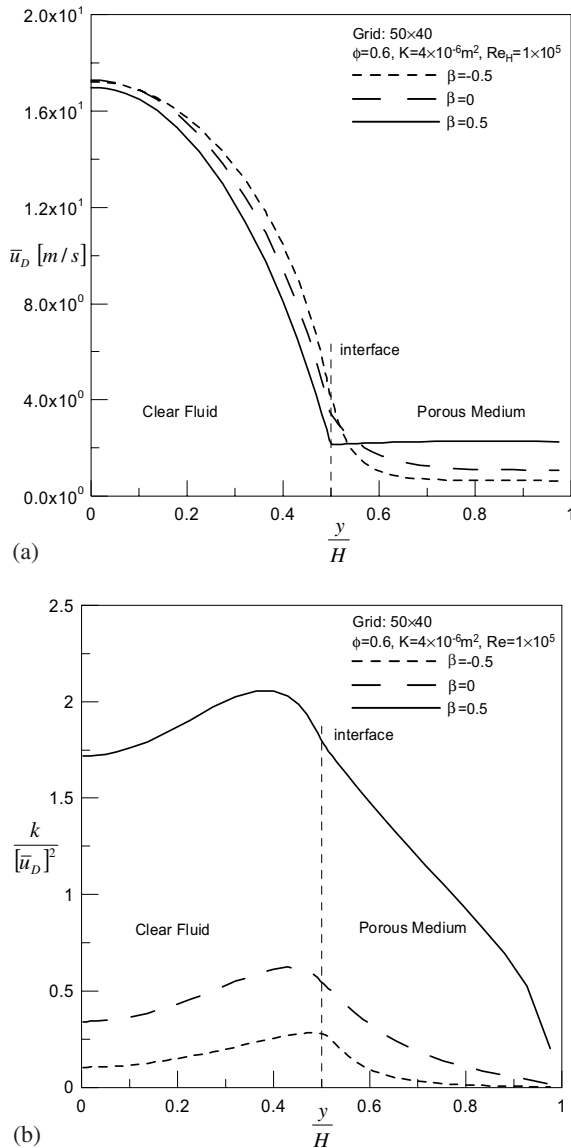


Fig. 7. Effect of parameter β on hydrodynamic field: (a) mean velocity, (b) turbulent field.

5. Concluding remarks

Numerical solutions for turbulent flow in composite channels were obtained for different values of Re_H , ϕ , K and β parameters. Results are coherent with model proposals for mean and turbulent fields. Although simulations were presented for one-dimensional flows, the implementation herein was done for two-dimensional situations and carried out on a generalized coordinate system. Future applications on natural environmental flows of interest, such as atmospheric boundary layer over rain forests, may bring insight on the determination of the overall exchange rates of energy [28] and mass transport [29] between the soil and the atmosphere.

Acknowledgements

The authors are thankful to CAPES and CNPq, Brazil, for their financial support during the course of this research.

References

- [1] S. Whitaker, *Advances in theory of fluid motion in porous media*, *Ind. Eng. Chem.* 61 (1969) 14–28.
- [2] W.G. Gray, P.C.Y. Lee, On the theorems for local volume averaging of multiphase system, *Int. J. Multiphase Flow* 3 (1977) 333–340.
- [3] J.A. Ochoa-Tapia, S. Whitaker, Momentum transfer at the boundary between a porous medium and a homogeneous fluid—I. theoretical development, *Int. J. Heat Mass Transfer* 38 (1995) 2635–2646.
- [4] J.A. Ochoa-Tapia, S. Whitaker, Momentum transfer at the boundary between a porous medium and a homogeneous fluid—II. Comparison with experiment, *Int. J. Heat Mass Transfer* 38 (1995) 2647–2655.
- [5] M.J.S. de Lemos, M.H.J. Pedras, Simulation of turbulent flow through hybrid porous medium–clear fluid domains, in: *Proc. of IMECE2000, ASME, Int. Mech. Eng. Congr., ASME-HTD-366-5*, Orlando, FL, 2000, pp. 113–122, ISBN 0-7918-1908-6.
- [6] M.H.J. Pedras, M.J.S. de Lemos, Macroscopic turbulence modeling for incompressible flow through undeformable porous media, *Int. J. Heat Mass Transfer* 44 (6) (2001) 1081–1093.
- [7] M.H.J. Pedras, M.J.S. de Lemos, Simulation of turbulent flow in porous media using a spatially periodic array and a low Re two-equation closure, *Numer. Heat Transfer Part A—Appl.* 39 (1) (2001) 35–59.
- [8] M.H.J. Pedras, M.J.S. de Lemos, On volume and time averaging of transport equations for turbulent flow in porous media, *ASME-FED*, vol. 248, Paper FEDSM99-7273, 1999, ISBN 0-7918-1961-2.
- [9] M.H.J. Pedras, M.J.S. de Lemos, On the definition of turbulent kinetic energy for flow in porous media, *Int. Commun. Heat Mass Transfer* 27 (2) (2000) 211–220.
- [10] F.D. Rocamora Jr., M.J.S. de Lemos, Analysis of convective heat transfer for turbulent flow in saturated porous media, *Int. Commun. Heat Mass Transfer* 27 (6) (2000) 825–834.
- [11] F.D. Rocamora Jr., M.J.S. de Lemos, Laminar recirculating flow and heat transfer in hybrid porous medium–clear fluid computational domains, in: *Proc. of 34th ASME-National Heat Transfer Conference (on CD-ROM), ASME-HTD-1463CD*, Paper NHTC2000-12317, Pittsburgh, PA, 2000, ISBN 0-7918-1997-3.
- [12] F.D. Rocamora Jr., M.J.S. de Lemos, Heat transfer in suddenly expanded flow in a channel with porous inserts, in: *Proc of IMECE2000, ASME, Int. Mech. Eng. Congr., ASME-HTD-366-5*, Orlando, FL, 2000, pp. 191–195, ISBN 0-7918-1908-6.
- [13] R.A. Silva, M.J.S. de Lemos, Laminar flow in a channel with a layer of porous material considering the non-linear Forchheimer term (in Portuguese), in: *II National Congress of Mechanical Engineering*, João Pessoa-PB, Brazil, 2002.
- [14] R.A. Silva, M.J.S. de Lemos, Flow in a channel partially filled with a porous material (in Portuguese), in: *Proc. of 16th Brazilian Congress of Mechanical Engineering (on CD-ROM)*, Uberlândia-MG, Brazil, 2001.
- [15] M.J.S. de Lemos, R.A. Silva, Numerical treatment of the stress jump interface condition for laminar flow in a channel partially filled with a porous material, in: *Proc. of ASME Fluids Eng. Div. Summer Meeting, Paper ASME-FEDSM2002-31126*, Montreal, Quebec, Canada, 2002.
- [16] A.V. Kuznetsov, Analytical investigation of the fluid flow in the interface region between a porous medium and a clear fluid in channels partially filled with a porous medium, *Int. J. Heat Fluid Flow* 12 (1996) 269–272.
- [17] A.V. Kuznetsov, Influence of the stresses jump condition at the porous-medium/clear-fluid interface on a flow at a porous wall, *Int. Commun. Heat Mass Transfer* 24 (1997) 401–410.
- [18] A.V. Kuznetsov, Fluid mechanics and heat transfer in the interface region between a porous medium and a fluid layer: a boundary layer solution, *J. Porous Media* 2 (3) (1999) 309–321.
- [19] R.A. Silva, M.J.S. de Lemos, Numerical analysis of the stress jump interface condition for laminar flow over a porous layer, *Numer. Heat Transfer Part A—Appl.* 43 (6) (2003) 603–617.
- [20] M. Prithiviraj, M.J. Andrews, Three-dimensional numerical simulation of shell-and-tube heat exchanger. Part I—Foundation and fluid mechanics, *Numer. Heat Transfer Part A—Appl.* 33 (1998) 799–816.
- [21] W.T. Sha, A new porous-media approach for thermal–hydraulic analysis, *Trans. ANS* 39 (1981) 510–512.
- [22] M. Kaviany, *Principles of Heat Transfer in Porous Media*, Springer, 1995.
- [23] K. Lee, J.R. Howell, Forced convective and radiative transfer within a highly porous layer exposed to a turbulent external flow field, in: *Proc. of the 1987 ASME–JSME Thermal Engineering Joint Conf.*, vol. 2, 1987, pp. 377–386.
- [24] S.N. Lane, R.J. Hardy, Porous rivers: a new way of conceptualising and modelling river and floodplain flows? in: D. Ingham, I. Pop (Eds.), *Transport Phenomena in Porous Media II*, first ed., Pergamon Press, 2002, pp. 425–449 (Chapter 16).
- [25] M.J.S. de Lemos, M.H.J. Pedras, Recent mathematical models for turbulent flow in saturated rigid porous media, *ASME J. Fluids Eng.* 123 (4) (2001) 935–940.
- [26] M.H.J. Pedras, M.J.S. de Lemos, On mathematical description and simulation of turbulent flow in a porous medium formed by an array of elliptic rods, *ASME J. Fluids Eng.* 123 (4) (2001) 941–947.
- [27] M.H.J. Pedras, M.J.S. de Lemos, Computation of turbulent flow in porous media using a low Reynolds $K-\epsilon$ model and an infinite array of transversally-displaced elliptic rods, *Numer. Heat Transfer Part A—Appl.* 43 (6) (2003) 585–602.
- [28] R.A. Silva, M.J.S. de Lemos, E.J. Braga, Modeling of turbulent natural convection in porous media, *Int. Comm. Heat Mass Transfer* 30 (5) (2003) 615–624.
- [29] M.J.S. de Lemos, M.S. Mesquita, Turbulent mass transport in saturated rigid porous media, *Int. Commun. Heat Mass Transfer* 30 (1) (2003) 105–113.